Supporting Information

Pilaz et al. 10.1073/pnas.0909894106

SI Results

Measuring Cell-Cycle Parameters in Synchronized Cell Populations. S-phase cumulative labeling is a well-validated technique for studying cell-cycle progression in asynchronous cycling populations (1). In a first instance, we attempted to use this technique to analyze the cell-cycle kinetics of the control and GOF electroporated precursors 24 h after electroporation. However, despite several attempts, the data failed to exhibit the normal linear increase in the proportions of EdU+ cells over time found either in nonelectroporated precursors (Fig. S1) (2–4) as well as in asynchronously cyling dissociated cell cultures (4). Instead, we observed extremely rapid and nonlinear increases followed by subsequent decreases in LI values during EdU exposure (Fig. S2 *A–C*). These data are not consistent with successive cohorts of cycling cells entering S phase and instead are suggestive of populations of synchronously cycling cells, the latter due to EGFP transfection occurring uniquely during a restricted portion of the cell cycle.

Transfection efficiency has been shown to vary significantly at different phases of the cell cycle. Efficiency is optimal during S, G2 and M phases and very poor during G1 phase (5, 6). It is hypothesized that transfection close to M phase is facilitated by nuclear membrane breakdown. The limiting factor for transfection efficiency, besides stability of transfected DNA, is not the DNA uptake in target cells but rather release from intracellular vesicles and transport to the nucleus where transcription takes place. In agreement with these considerations, we found that precursors expressing EGFP immediately after electroporation (8 h is the minimal time for EGFP expression to be detectable) are predominantly cells that are in S, G2/M phases at the time of electroporation (Fig. 1*C*). Pulse injection of EdU made 30 min before electroporation returned approximately 74% of EdU+ EGFP+, confirming that the initially transfected population was almost entirely contained in the S and G2/M phases. EdU or BrdU pulse injections performed 4 h and 8 h after electroporation show a sharp decrease in the proportion of double-labeled cells (42 and 0% respectively) (Fig. S1 *C–E*), indicating that the plasmid is viable in the cells for <8 h. In agreement with data from synchronous cell lines (6) this shows that electroporation-mediated transfection in the VZ targets a synchronized cohort of cycling precursors. These findings caution on indiscriminative use of S-phase labeling and cumulative S-phase labeling as a means of measuring cell-cycle phases in electroporated cells.

Experimental Strategy to Reduce TG1. The progression through the G1 phase is under the control of cyclin-dependent kinases (cdks), and their binding partners, D-type cyclins and E-type cyclins. During early G1 phase cdk4 and/or cdk6 are activated by D-type cyclins. In the late G1 phase, cdk2 is activated by binding to cyclin E1 (7, 8). Given that cyclin D1 overexpression has been shown to induce cyclin E synthesis, via its action on E2F (9), we first expected cyclin D1 to have a more powerful effect on cell-cycle progression than cyclin E1. However, cyclin D1 acts outside of cell-cycle progression, which could constitute confounding effects for the present investigation. For instance, it has been shown that in addition to their established role in regulating the activity of cdk4/6, D-type cyclins can modify the activity of certain transcription factors (10) and noticeably repress bHLH proteins that are important for inducing terminal differentiation (11–14). Cyclin E1 is known to have less pleiotropic effects and is therefore predicted to exert a more straightforward role on a primary aim of the present study (examining the impact of TG1 on mode of division). However, cyclin E has been shown to influence the fate of the progeny of proliferative divisions in *drosophila* thoracic neuroblasts (15). If operant in cortical neuroblasts, such an effect on cell fate could also influence the results of the present study.

Modeling of the Impact of TG1 Variations on Neuron Production and Layer Formation. We have used a compartmentalized model of corticogenesis (16). Initial number of precursors (P) was identical in each condition. Tc values were ranging from 8 h (E11) to 18 h (E19). A reduction of 4 h in Tc and an 87% increase in cell-cycle reentry have been implemented in 30% of the E15 precursor pool, from E15 to E17. The simulation shows that the major increase in the size of the precursor pool is induced by the variation of cell-cycle reentry. Tc variation alone cannot account for the increase observed in vivo (Fig. S8*F*). Although we observe a good match between the observed and predicted variations of neuron density in the different layers subsequent to induced modifications of TG1, there are slight discrepancies in the magnitude of the variations. The experimental data (Fig. 4*E*) return smaller variations than the modeling predictions (Fig. S8 *A–D*). Whereas the model predicts an increase of 28% in the supragranular layers neuron number, the observed increase is smaller (10%). The magnitude is also reduced in layer 5 where the experimental observations return a nonsignificant 3–4% decrease in cell density to be compared to the 16% predicted decrease in neuron number. These discrepancies reflect the limitations of the model which does not take into account the magnitude of the dispersal or tangential spread required during the formation of the cortical plate and the full differentiation of the neuropile (17). Both factors lead to wider internuclear distances that will influence cell density measurements. Nevertheless, this model is sufficiently realistic given that the control situation generates the adequate proportions of neurons in each of the 6 layers (16, 18)

SI Methods

Preparation of Brain Sections. Embryonic brains were dissected in PBS and were then fixed by immersion in cold buffered 4% paraformaldehyde (PFA) in 120 mM phosphate buffer overnight. Coronal cryosections (20-μm) were made after cryoprotection in 20% sucrose overnight and embedded in Tissue-Tek, mounted on glass slides and stored at −40 °C. For fixation of postnatal brains, intracardiac perfusion of PBS (5 min) was followed by perfusion of 4% PFA (10 min). After post-fixation in 4% PFA overnight, brains were cryoprotected in 20% sucrose and frozen by exposition to isopentane (−40 °C) in liquid nitrogen. Forty-micrometer-thick coronal sections were made and stored in a buffered sodium azide solution.

Immunofluorescence and Antibodies. Sections were air-dried for 30 min and hydrated in Tris-buffered saline (TBS) for 30min. Glass slides were rinsed three times in TBS + Triton (0.5%) and incubated in normal goat serum (10%) + BSA (BSA, 1%) in TBS for 30 min. Primary antibodies were coincubated overnight in BSA (1%) in TBS at 4 °C as follows: rabbit anti-cyclin E1 (clone Ab-1, Neomarkers, 1:200), rabbit anti-GFP coupled with alexa 488 (Invitrogen 1:1,000), rabbit anti-Tbr2 (Abcam, 1:1,000), rabbit anti-Cux1 (clone M-222, Santa Cruz, 1:200), rabbit anti-phosphorylated histone H3 (pH3, Ser-28, Upstate, 1:200), rabbit anti-cyclin D1 (SP4, Neomarkers, 1:200), mouse anti-Pax6 (Developmental Studies Hybridioma Bank, 1:1,000),

mouse anti-Ki67 (clone MM1, Dako, 1:100), rat anti-BrdU (clone BU1/75, Abcam, 1:200), rat anti-Ki67 (clone TEC-3, Dako, 1:50), chicken anti-GFP (Abcam, 1:1,000).

For Pax6 and Ki67 staining, heat-mediated antigen retrieval was performed for 10 min at 95 °C in a Dako antigen retrieval reagent before incubation in normal goat serum. For BrdU staining, sections were incubated in 2 N HCl for 30 min at 37 °C, followed by incubation in sodium borate (pH 8.5) for 15 min twice. EdU revelation was performed by using the EdU Click-iT EdU Alexa Fluor 594 (or 647) Kit according to the manufacturer's recommendations.

Counting of Cell Types. All cell countings were made without the experimenter knowing the identity of the transfection condition. Images were collected by confocal microscopy by using LCS software (Leica) with a 40× oil objective, and consisted of the projection of several focal planes acquired over a 3- to 5-μm depth. When the regions of interest covered more than one optical field, reconstructions were made by using the Adobe Photoshop Software. Brightness and contrast were adjusted and the cells were counted by using the Cell Counter Plugin in ImageJ (19). The boundaries between different compartments were based on cytological cues and differential immunoreactivity to different proteins (Fig. S9).

Organotypic Slice Culture and Bi-Photon Imaging. To perform real-time imaging of electroporated cycling precursors, mouse embryos were electroporated in utero at E15. Sixteen hours after electroporation, acute brain slices [coronal, 150 μm, vibratome (Leica VT1000S)] were prepared. The slices were cultured in a Millicell culture insert system (Millipore) in GMEM supplemented with, 1% sodium pyruvate, 1% nonessential amino acids, 2 mM glutamine, 1% penicillin/streptomycin, and 10% FCS for 5 h before time-lapse. Two-photon time-lapse video recordings were performed by using an inverted Axio-Observer Z1 (Zeiss) two-photon microscope, equipped with a Chameleon system Ultra (I) Titane Sapphire 80 Mhz laser tuned to 880 nm for GFP imaging, and an apochromatic dry objective 10×/0.45. The recording system is equipped with a Microscope Cage Incubation System (Okolab) maintaining temperature at 37 °C and CO_2 at 7.5% during the whole recording session. By using the multiposition Zeiss LSM 510 software, 4D stacks are acquired every 30 min, between 16 and 72 h after electroporation, on a 100-μm thickness (20 optical sections spaced at 5-μm intervals). Manual tracking of cell movements and divisions was done by the experimenter by using the ImageJ software.

BrdU and EdU Labeling. For in vivo labeling of S phase cells, a single i.p. injection of BrdU (50 μg/g diluted in PBS) or EdU (2.5 mg/mL, 150 μL diluted in PBS) was performed at different time points relative to sacrifice or electroporation. BrdU-positive and EdU-positive cells were detected by immunohistochemistry as described above.

Cumulative BrdU or EdU Labeling. The protocol was carried out via repeated i.p. injections, performed at different time-intervals. In the in vivo cumulative EdU protocol, EdU was administered to the pregnant mouse at E16, starting 20 h after in utero electroporation of plasmids at E15. In the ex vivo cumulative BrdU protocol, the beginning of BrdU exposure started few hours after ex utero electroporation, and at the beginning of slice culture.

Apoptosis. The ApopTag kit (Millipore) was used according to the manufacturer recommendation to detect apoptotic cells in the electroporated region of E17 brain, 48h after electroporation.

Confocal Measurements of GFP, Cyclin E1, Cyclin D1 Expression Levels. We have quantified protein expression levels by means of confocal microscopy analysis of immunofluorescent labeling (20–22). Confocal examination of the fluorescent labeling was carried out on a LEICA TCS SP equipped with an Argon-krypton laser. Several fields of view were analyzed so as to span the entire thickness of the GZ. The expression levels were analyzed at the single cell level in the EGFP expressing precursors on 20 microns thick sections. Analysis of cyclin E1 and cyclin D1 overexpression was performed by using a 40× oil objective. Quantitative analysis of alexa 555 fluorescence in the GFP+ cells was performed by using ImageJ.

Statistical Analysis. Quantitative data are presented as the mean ± SEM. from representative experiments. The experiments were repeated at least three times. Statistical tests used to compare data and their returned P values are indicated in the figure legends. Student t tests were performed (when dealing with numerical values) with the Excel software and GLM analysis (when dealing with percentages) with the R software (23). The boxplot analysis (24), was performed with the R software. $P < 0.05$ was considered statistically significant.

Mathematical Modeling. We used a deterministic, compartmentalized model of corticogenesis. The compartmental model is based on a linear ordinary differential (ODE) equations system (16, 25). The use of compartments provides a powerful tool to simulate transitions of cells from one state to another as a function of time.

The model design includes four compartments: (*i*) compartment containing cycling progenitors (Pcycling), (*ii*) compartment containing progenitors that are at the end of the mitosis (Pend.of.mitosis), (*iii*) compartment of postmitotic neurons, and (*iv*) compartment containing the total number of neurons in each layer (Layer i). Lpi(t) is the fraction of neurons produced at a time t that will be allocated to the layer i. (i = 1…5).

ODE equations:

$$\frac{dP_{cycling}}{dt} = (1 - LF(t)) \times P_{end.of.mitosis} - \frac{ln(2)}{Tc(t)} \times P_{cycling} \quad [1]$$

$$\frac{dP_{end.of.mitosis}}{dt} = 2 \times \frac{ln(2)}{Tc(t)} \times P_{cycling} - P_{end.of.mitosis} \quad [2]$$

$$\frac{dNeurons}{dt} = LF(t) \times P_{end.of.mitosis} \quad [3]$$

$$\frac{dLayer_i}{dt} = Lp_i(t) \times LF(t) \times P_{end.of.mitosis} \quad [4]$$

Tc is the cell cycle duration and LF is the leaving fraction (i.e., 1—cell-cycle reentry fraction). Biological data corresponding to these two parameters for area 3 of the somatosensory cortex can be found in refs. 16 and 26.

The simulation begins at E11 and terminates at E18.5. For the GOF experiment modeling, the modifications of Tc and LF have been implemented in 30% of the precursor population (corresponding to the transfection rate), from E15 to E17.

1. Nowakowski RS, Lewin SB, Miller MW (1989) Bromodeoxyuridine immunohistochemical determination of the lengths of the cell cycle and the DNA-synthetic phase for an anatomically defined population. *J Neurocytol* 18:311–318.
2. Calegari F, Haubensak W, Haffner C, Huttner WB (2005) Selective lengthening of the cell cycle in the neurogenic subpopulation of neural progenitor cells during mouse brain development. *J Neurosci* 25:6533–6538.
3. Dehay C, Savatier P, Cortay V, Kennedy H (2001) Cell-cycle kinetics of neocortical precursors are influenced by embryonic thalamic axons. *J Neurosci* 21:201–214.

4. Fluckiger AC, et al. (2006) Cell cycle features of primate embryonic stem cells. *Stem Cells* 24:547–556.
5. Brunner S, et al. (2000) Cell cycle dependence of gene transfer by lipoplex, polyplex and recombinant adenovirus. *Gene Ther* 7:401–407.
6. Grosjean F, Batard P, Jordan M, Wurm FM (2002) S-phase synchronized CHO cells show elevated transfection efficiency and expression using CaPi. *Cytotechnology* 38:57–62.
7. Sherr CJ, Roberts JM (1999) CDK inhibitors: Positive and negative regulators of G1-phase progression. *Genes Dev* 13:1501–1512.
8. Sherr CJ, Roberts JM (2004) Living with or without cyclins and cyclin-dependent kinases. *Genes Dev* 18:2699–2711.
9. Resnitzky D, Reed SI (1995) Different roles for cyclins D1 and E in regulation of the G1-to-S transition. *Mol Cell Biol* 150:3463–3469.
10. Coqueret O (2002) Linking cyclins to transcriptional control. *Gene* 299:35–55.
11. Inoue K, Sherr CJ (1998) Gene expression and cell cycle arrest mediated by transcription factor DMP1 is antagonized by D-type cyclins through a cyclin-dependent-kinase-independent mechanism. *Mol Cell Biol* 18:1590–1600.
12. Rao SS, Chu C, Kohtz DS (1994) Ectopic expression of cyclin D1 prevents activation of gene transcription by myogenic basic helix–loop–helix regulators. *Mol Cell Biol* 14:5259–5267.
13. Ratineau C, Petry MW, Mutoh H, Leiter AB (2002) Cyclin D1 represses the basic helix–loop–helix transcription factor, BETA2/NeuroD. *J Biol Chem* 277:8847–8853.
14. Skapek SX, Rhee J, Spicer DB, Lassar AB (1995) Inhibition of myogenic differentiation in proliferating myoblasts by cyclin D1-dependent kinase. *Science* 267:1022–1024.
15. Chia W, Somers WG, Wang H (2008) *Drosophila* neuroblast asymmetric divisions: Cell cycle regulators, asymmetric protein localization, and tumorigenesis. *J Cell Biol* 180:267–272.
16. Polleux F, Dehay C, Moraillon B, Kennedy H (1997) Regulation of neuroblast cell-cycle kinetics plays a crucial role in the generation of unique features of neocortical areas. *J Neurosci* 17:7763–7783.
17. Lukaszewicz A, et al. (2006) The concerted modulation of proliferation and migration contributes to the specification of the cytoarchitecture and dimensions of cortical areas. *Cereb Cortex* 16:i26–34.
18. Skoglund TS, Pascher R, Berthold CH (1996) Heterogeneity in the columnar number of neurons in different neocortical areas in the rat. *Neurosci Lett* 208:97–100.
19. Abramoff MD (2004) Image processing with ImageJ. *Biophotonics International* 11:36–42.
20. Durand B, Gao FB, Raff M (1997) Accumulation of the cyclin-dependent kinase inhibitor p27/Kip1 and the timing of oligodendrocyte differentiation. *EMBO J* 16:306–317.
21. Lukaszewicz A, Savatier P, Cortay V, Kennedy H, Dehay C (2002) Contrasting effects of basic fibroblast growth factor and neurotrophin 3 on cell cycle kinetics of mouse cortical stem cells. *J Neurosci* 22:6610–6622.
22. Tokumoto YM, Apperly JA, Gao FB, Raff MC (2002) Posttranscriptional regulation of p18 and p27 Cdk inhibitor proteins and the timing of oligodendrocyte differentiation. *Dev Biol* 245:224–234.
23. Team RDC (2008) *R: A Language and Environment for Statistical Computing* (Vienna, Austria).
24. Tukey JW (1977) *Explanatory Data Analysis* (Redding, MA).
25. Lander AD, Gokoffski KK, Wan FY, Nie Q, Calof AL (2009) Cell lineages and the logic of proliferative control. *PLoS Biol* 7:e15.
26. Takahashi T, Nowakowski RS, Caviness VSJ (1995) The cell cycle of the pseudostratified ventricular epithelium of the embryonic cerebral wall. *J Neurosci* 15:6046–6057.

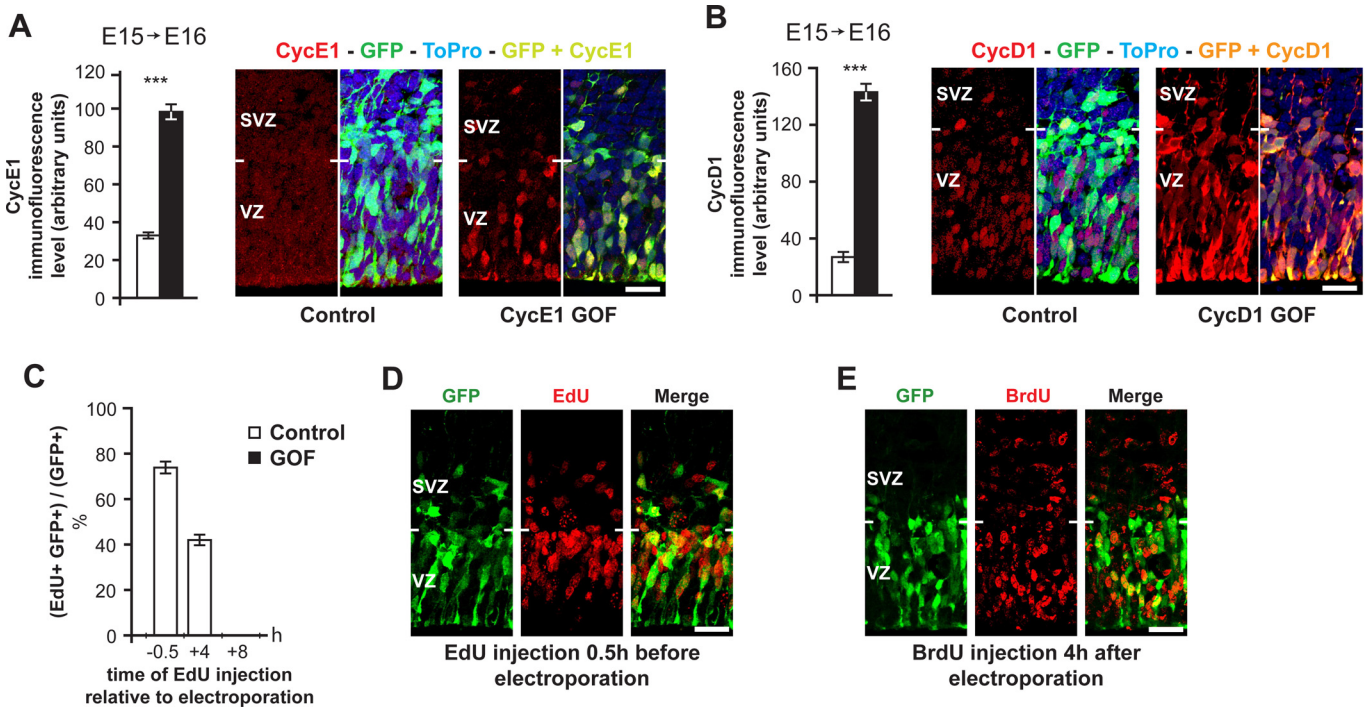

Fig. S1. Induced cyclin E1 and cyclin D1 overexpression in the electroporated precursors and their progeny. (*A*) Confocal microscopy quantification of the intensity of the fluorescent immunolabeling against cyclin E1 in the EGFP+ precursors of the GZ, 24 h after electroporation (the antibody recognizes both human and mouse cyclin E1). (*B*) Confocal microscopy quantification of the intensity of the fluorescent immunolabeling against cyclin D1 in the EGFP+ precursors of the GZ, 24 h after electroporation. Unpaired *t* test CycE1 GOF: $P < 0.001$; CycD1 GOF: $P < 0.001$. (*C–E*) Electroporation targets a cohort of cycling precursors in *S*, G2/M phases (*C*) Percentage of transfected cells that have incorporated BrdU at different time intervals before and after electroporation. (*D* and *E*) Confocal microphotographs showing EdU and BrdU incorporation in the EGFP+ electroporated precursors. (Scale bars, 33 μm.)

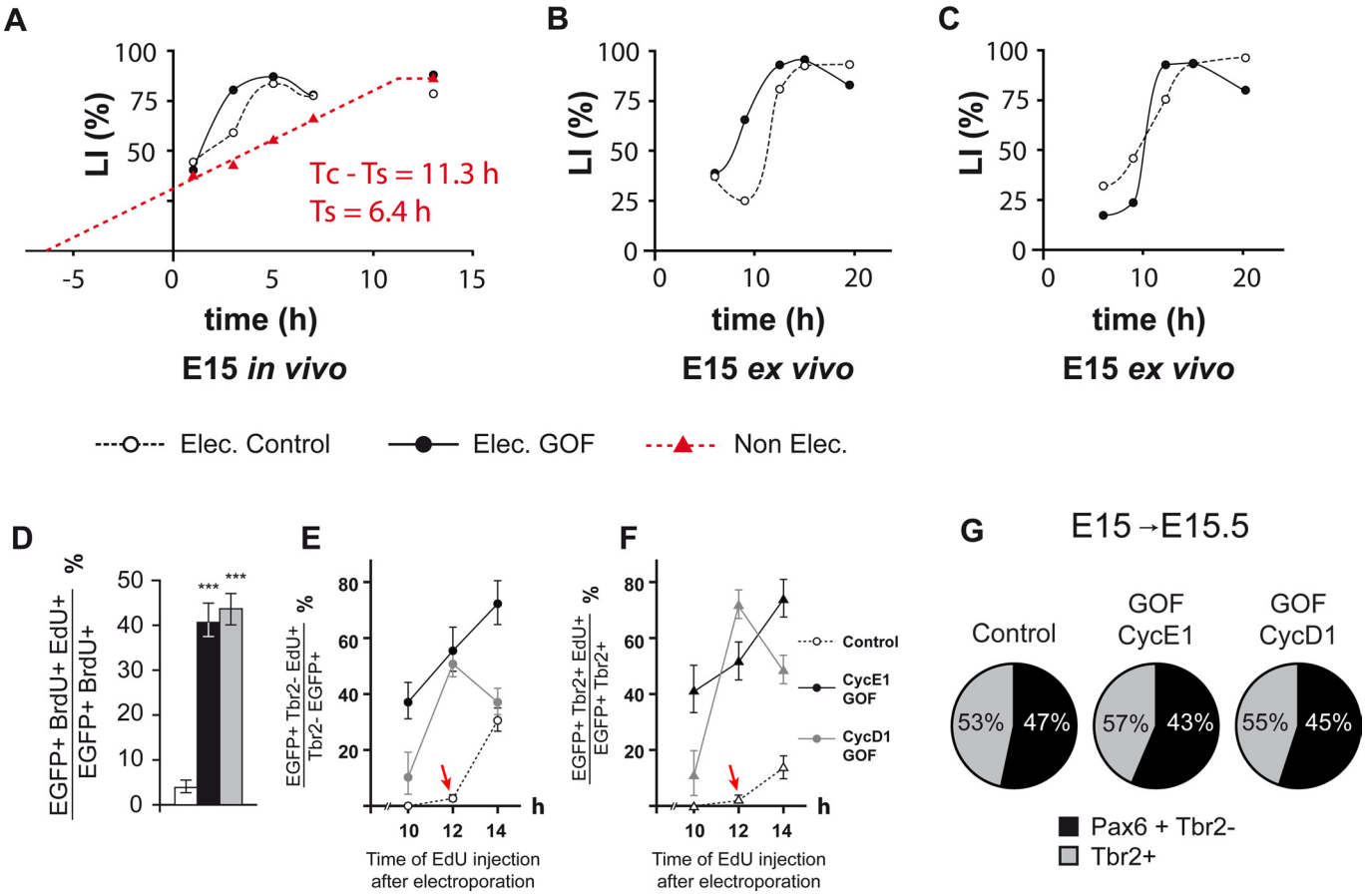

Fig. S2. S-phase cumulative labeling in electroporated and nonelectroporated precursors. (*A*) EdU cumulative labeling in nonelectroporated precursors show a linear increase in the LI values, as described previously in numerous studies. The linear increase in LI is due to asynchronous cohorts of cells entering S phase and returns Tc values of 17 h and Ts of 6.4 h. By contrast, in both control electroporated (from the same sections) and GOF electroporated precursors, the LI increase upon time of exposure was not linear and reached a maximum at 5 h. The slope of the ascending curve is steep and its extrapolation on the negative arm of the *x* axis, used to define Ts, would lead a nonexisting S phase in the electroporated control precursors. (*B* and *C*) Additional examples of BrdU cumulative labeling on organotypic slices at E16, after electroporation at E15. Note the nonlinear and rapid increase in LI values. (*D*) Double S-phase labeling: EGFP+ BrdU+ cells correspond to the electroporated precursors in S phase at the time of electroporation, and EGFP+ EdU+ cells to cells in S phase 12 h after electroporation. GLM analysis: cyclin E1 GOF: $P < 0.001$; cyclin D1 GOF: $P < 0.001$. (*E*) TG1 in GOF and control transfected Tbr2-precursors in the VZ. An increasing proportion of EdU+/EGFP+ cells are detected in both GOF conditions, 10 h and 12 h after electroporation, whereas the first EDU+/EGFP+ precursors are detected only 12 h (red arrow) after electoporation in control precursors. (*F*) TG1 in GOF and control transfected Tbr2+ precursors in the VZ and SVZ. EdU+/EGFP+ cells are detected 10 h after electroporation in both GOF conditions, whereas the first EDU+/EGFP+ precursors are detected only 12 h (red arrow) after electoporation in control precursors. (*G*) Percentage of Tbr2+ and Pax6+ Tbr2- cells in the EGFP expressing cells. Immunostaining against Pax6 and Tbr2 was performed 12 h after electroporation at E15.

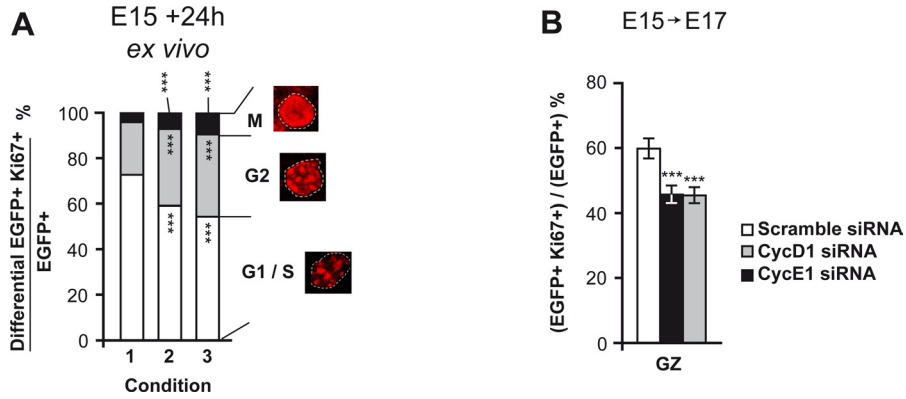

Fig. S3. Analysis of cell-cycle-phase-related differential expression of Ki67 in GOF and control transfected precursors. (*A*) The qualitative aspect of the Ki67 staining differs between cell-cycle phases. The proportions of precursors exhibiting dense punctuate staining (G2 phase), sparse punctuate staining (G1/S phases) and dense uniform labeling (M phase) were observed 24 h after electroporation, on organotypic slices of E16 cortex. The proportion of precursors exhibiting a nuclear Ki67 punctuate staining is lower in GOF precursors, indicating a shorter G1 phase. Conditions 1, 2, and 3 correspond to control, GOF cyclin E1 and GOF cyclin D1, respectively. (*B*) Percentage of cycling cells in the transfected populations and their progeny after siRNA targeting cyclin D1 transfection, as shown by Ki67 expression. Measurements were made in the GZ in vivo, at 48 h after electroporation at E15. GLM analysis: CycE1 siRNA: $P < 0.001$; CycD1 siRNA: $P = 0.00021$.

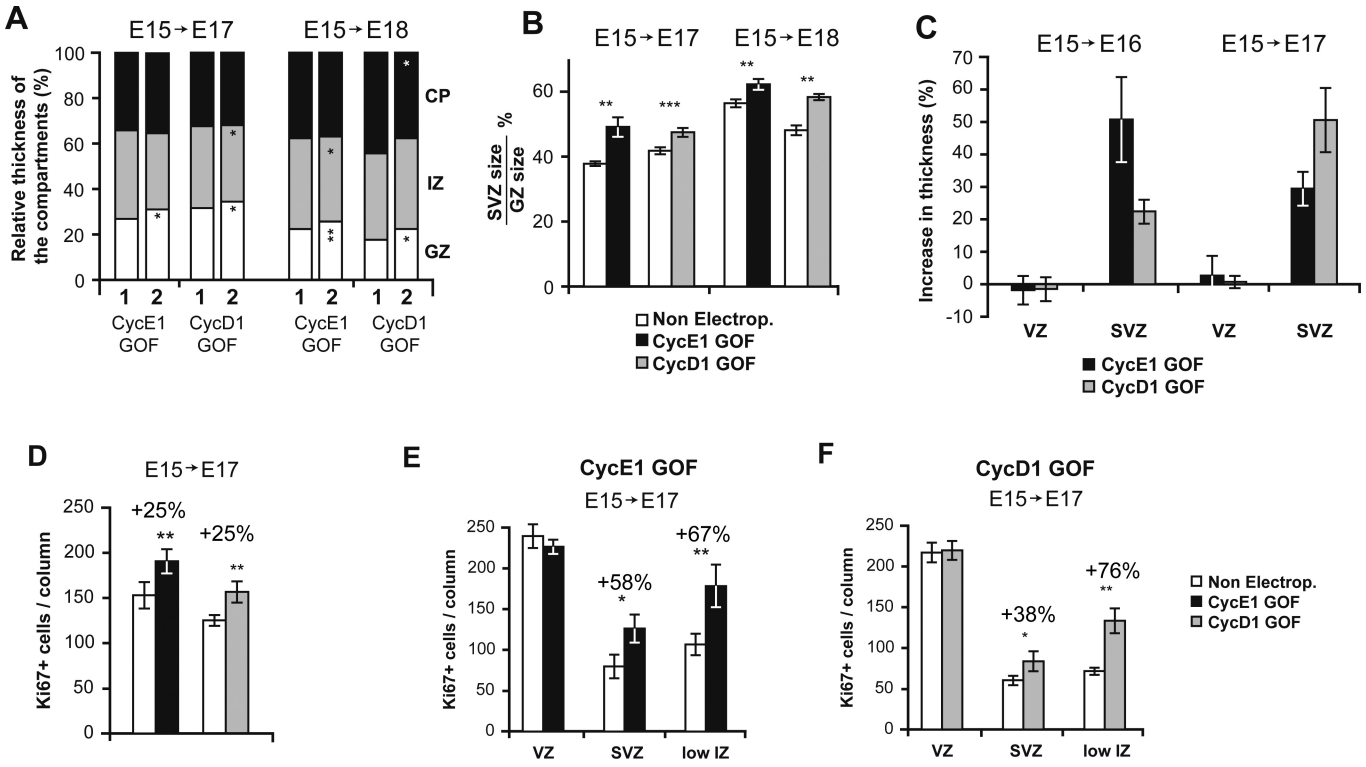

Fig. S4. Consequence of GOF on the size of germinal compartments. (*A*) Relative thickness of the GZ and postmitotic compartments measured in the electoporated regions at E17 and E18. ''2'' corresponds to the electroporated region and ''1'' to the contralateral nonelectroporated region on a same section. Paired Student *t* test: E15–E17 cyclin E1 GOF: $P = 0.029$; E15–E17 cyclin D1 GOF: $P = 0.015$; E15–E18 cyclin E1 GOF: $P = 0.0034$; E15–E18 cyclin D1 GOF: $P = 0.013$. (*B*) Increase in the relative thickness of the SVZ in GOF conditions compared to controls. Paired *t* test: E15–E17 cyclin E1 GOF: $P = 0.0091$; E15–E17 cyclin D1 GOF: $P = 0.00076$; E15–E18 cyclin E1 GOF: $P = 0.0013$; E15–E18 cyclin D1 GOF: $P = 0.0010$. (*C*) Increase in the absolute size of the SVZ in GOF conditions compared to control. The thickness of the VZ and the SVZ were measured on coronal sections in the electroporated region and compared to the strictly homologous region of the opposite nonelectroporated hemisphere. (*D*) Number of Ki67+ cells in a 100-μm wide column of E17 cortices in GOF electroporation. Paired *t* test: cyclin E1 GOF: $P = 0.00084$; cyclin D1 GOF: $P = 0.0040$. (*E* and *F*) Number of Ki67+ cells counted in a 100-μm wide column, after cyclin E1 or cyclin D1 GOF electroporation at E15. The control is the strictly homologous region of the nonelectroporated hemisphere. Paired *t* test: SVZ cyclin E1 GOF: $P = 0.032$; SVZ cyclin D1 GOF $P = 0.031$; DMC cyclin E1 GOF: $P = 0.070$; DMC cyclin D1 GOF: $P = 0.063$.

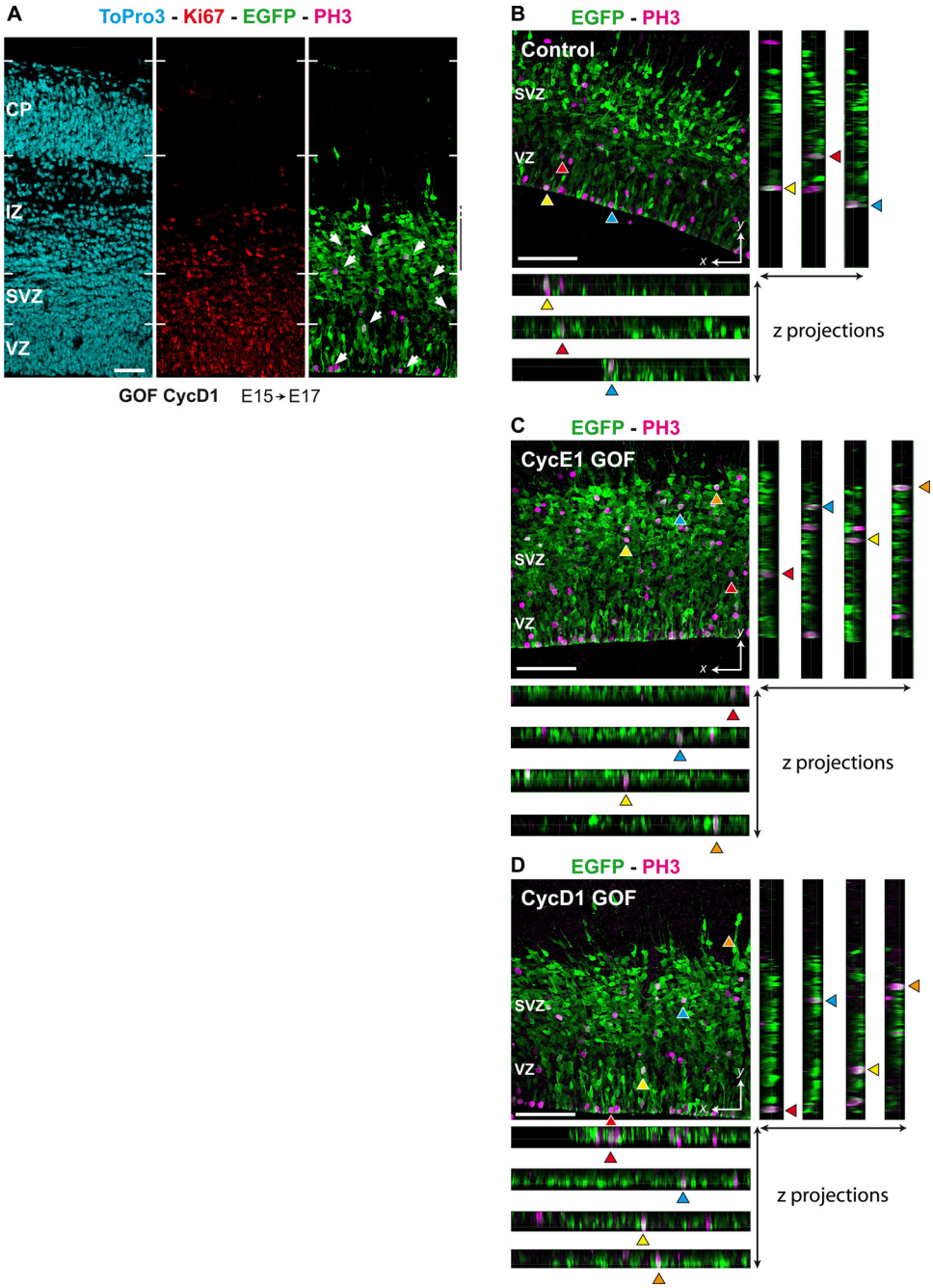

Fig. S5. (*A*) Confocal microphotographs of coronal sections showing Ki67 and PH3 expressing cells in the electoporated regions of a GOF cyclin D1 E17 brain, after electroporation at E15. (Scale bar, 50 μm.) (*B–D*) 3D confocal analysis of EGFP and PH3 immunostained coronal sections asserting colocalisation of EGFP and PH3 signals shown in Fig. 3 *A* and *B*, *Right* and Fig. S4 *Right*. EGFP and PH3 colocalisation appears in white and is indicated by arrowheads. Signal z-cut reconstruction along the *x* and the corresponding *y* axis are shown in the *Bottom* and *Right*, respectively. (Scale bar, 100 μm.)

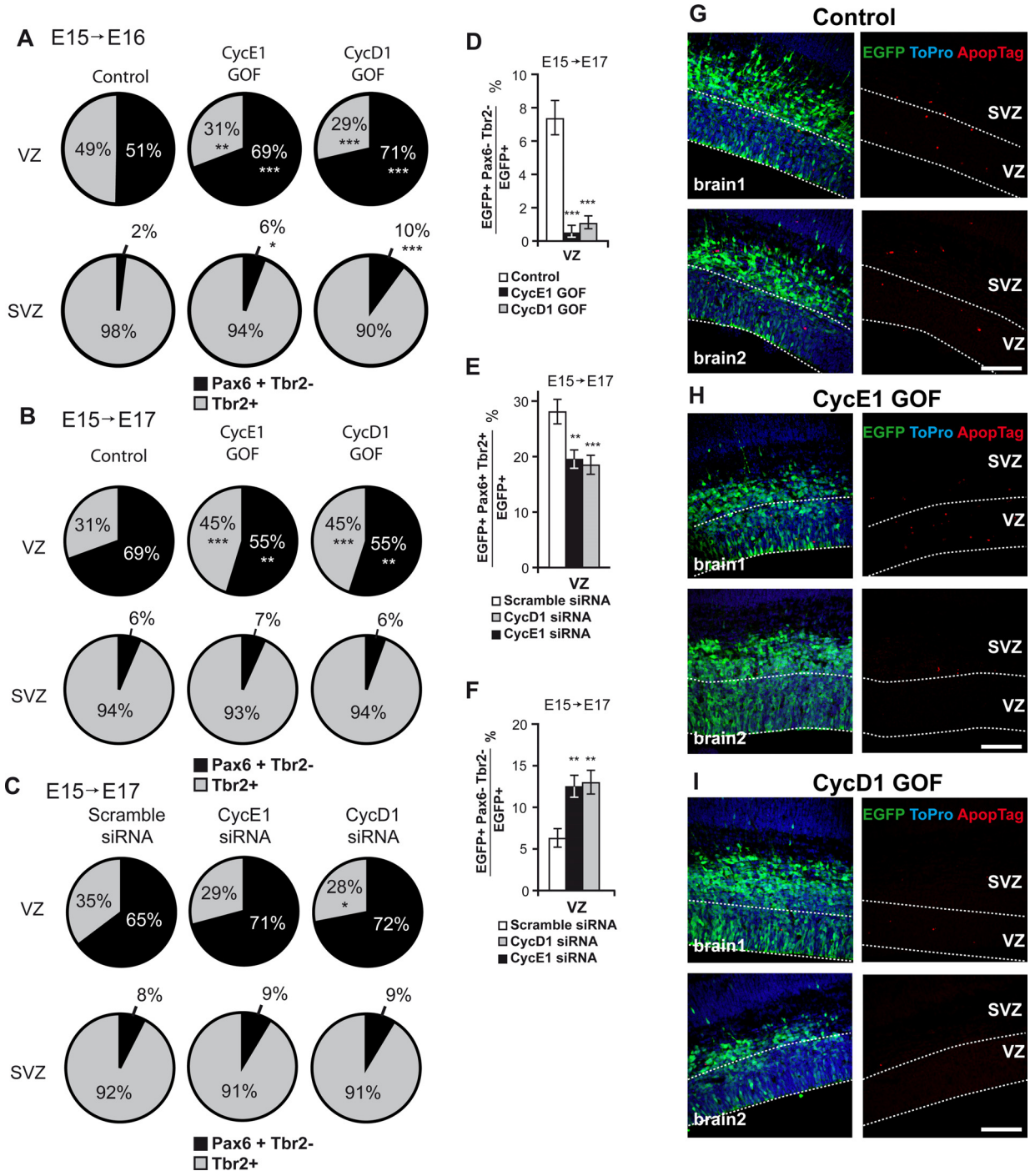

Fig. S6. Consequence of GOF and down-regulation on precursor pools. (*A*) Overexpression of cyclin D1 and cyclin E1 led to a statistically significant increase in the proportion of Pax6+ progenitors in the electroporated populations at E16 (statistical difference in the VZ: GOF CycE1: $P = 0.00012$; GOF CycD1: $P < 0.001$ GLM analysis). (*B*) Overexpression of cyclin D1 and cyclin E1 led to a statistically significant increase in the proportion of Tbr2+ progenitors in the electroporated populations at E17 (statistical difference in the VZ: GOF CycE1: $P = 0.00012$; GOF CycD1: $P < 0.001$ GLM analysis). Overexpression of cyclin D1 and cyclin E1 did not modify the proportion of Pax6 and Tbr2 expressing precursors in the SVZ (GLM analysis: GOF CycE1: $P = 0.94$; GOF CycD1: $P = 0.91$). (*C*) Down-regulation of cyclin E1 and cyclin D1 leads to a reduction in the proportion of Tbr2+ progenitors in the electroporated populations at E17. GLM analysis: CycE1 siRNA: $P = 0.19$; CycD1 siRNA: $P = 0.0018$. (*D*) Forced expression of cyclin E1 and cyclin D1 induces a reduction of Pax6-Tbr2- proportions in the electroporated populations in the VZ at E17. GLM analysis: GOF CycE1: $P < 0.001$; GOF CycD1: $P < 0.001$. (*E*) Down-regulation of cyclin E1 and cyclin D1 induces a decrease of Pax6+Tbr2+ proportions in the VZ at E17. GLM analysis: CycE1 siRNA: $P < 0.001$; CycD1 siRNA: $P < 0.001$. (*F*) Down-regulation of cyclin E1 and cyclin D1 induces an increase of Pax6-Tbr2- proportions in the VZ at E17. GLM analysis: CycE1 siRNA: $P = 0.032$; CycD1 siRNA $P = 0.029$. (*G–I*) Confocal microphotographs of coronal sections at E17 showing EGFP, Topro3 and ApopTag immunostaining in two different brains for each condition. No difference in apoptosis rates are observed between control and GOF conditions. (Scale bar, 100 μm.)

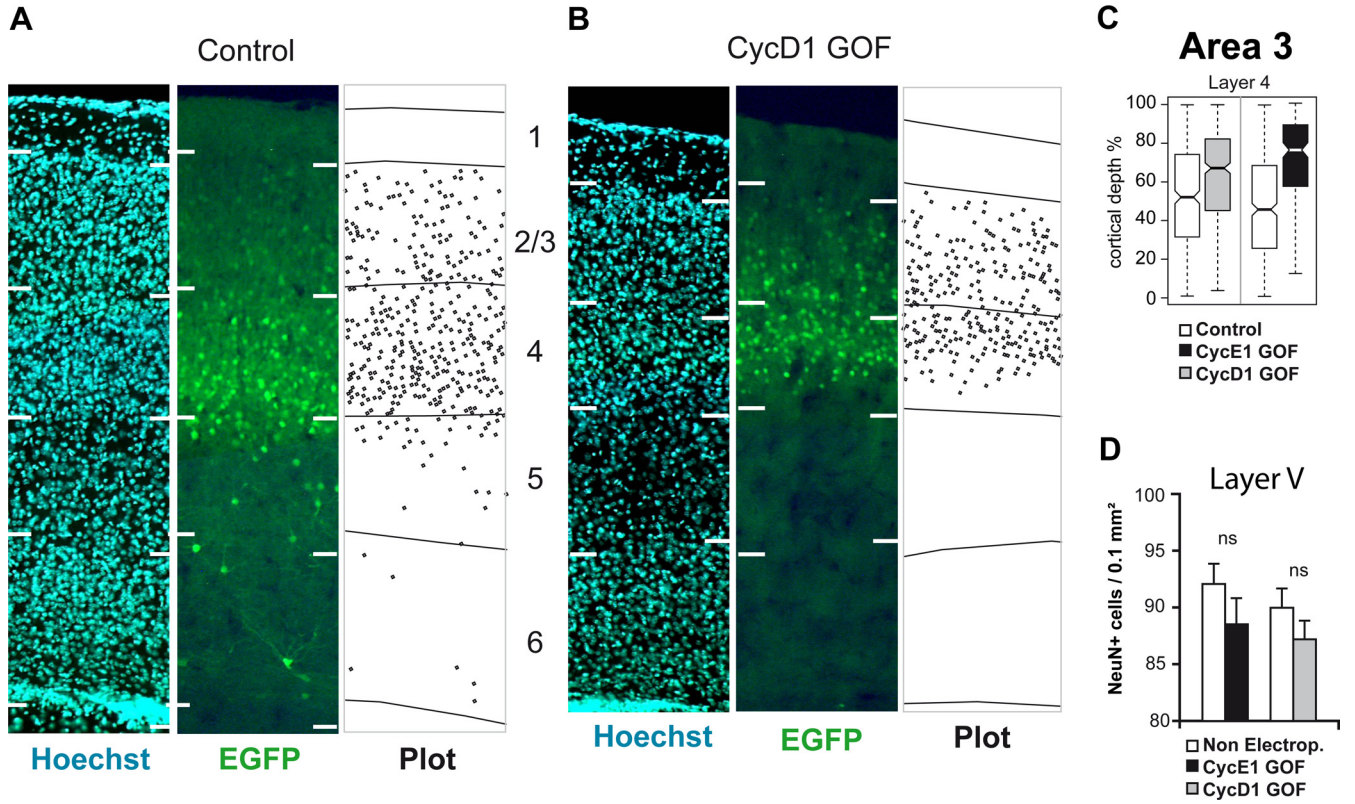

Fig. S7. Laminar phenotype of post-mitotic neurons generated by the transfected precursors, 2 weeks after birth, in control and GOF conditions. (*A* and *B*) Photomicrographs of a transect of Hoechst and EGFP stained coronal section in area 3 showing the limits of plots of the distribution of EGFP expressing neurons born from control (*A*) and GOF (*B*) precursors. (Scale bar, 100 μm.) (*C*) Box plot analysis of the radial distribution of layer 4 EGFP neurons, born from control and GOF precursors in area 3. Individual box indicates mid-50th percentile range of individual distance neuron measurements. Whiskers, tenth to ninetieth percentiles; horizontal bold line, mean. (*D*) Variations in neuron density in layer 5 of area 3 in the electroporated region compared to control, at P15. Paired *t* test: cyclin E1 GOF: $P = 0.203$; cyclin D1 GOF: $P = 0.609$. No statistical difference in neuron density was observed between nonelectroporated and control electroporated regions.

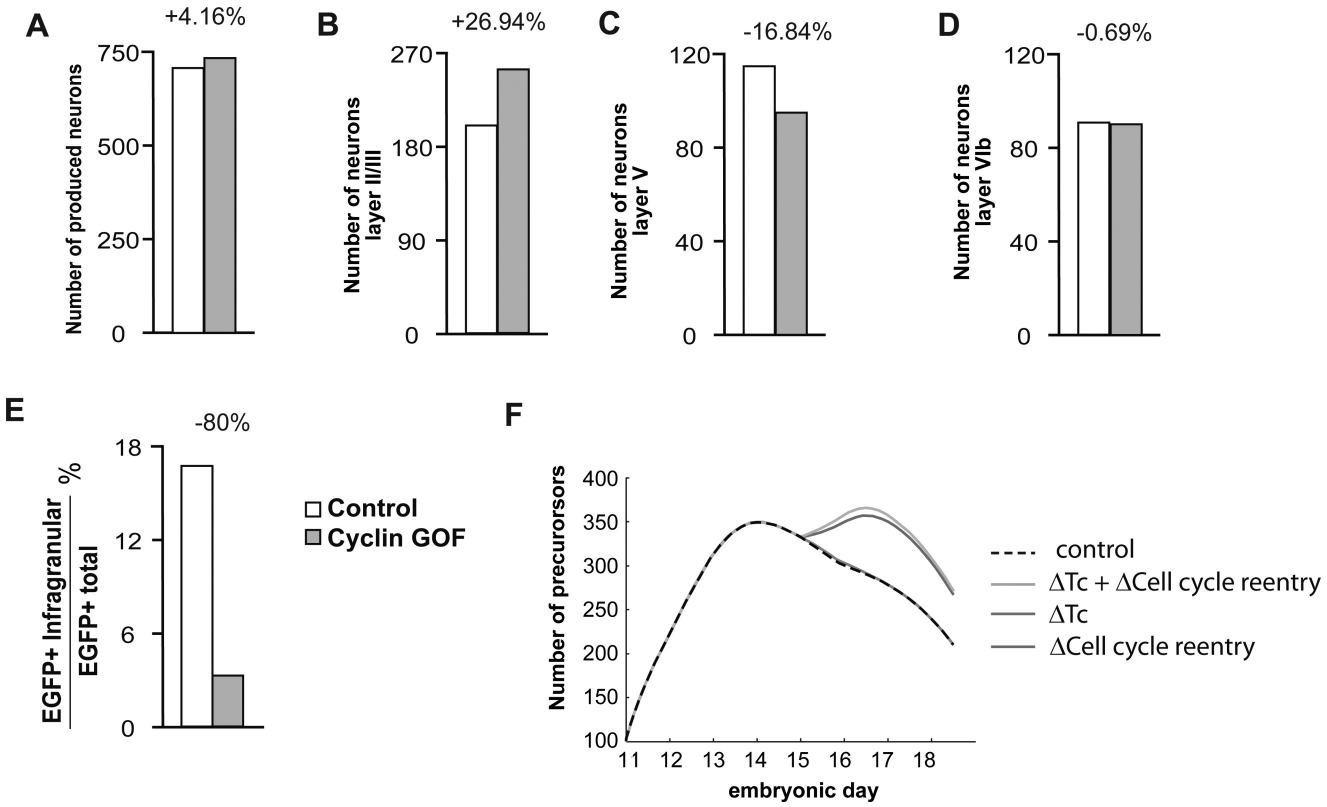

Fig. S8. Modeling of the impact of TG1 variations on neuron production and layer formation. (*A*) GOF induced changes in Tc and cell-cycle reentry (*Q*) generate a 4% difference in the total number of neurons produced. (*B*) Number of layer 2 and 3 neurons produced in GOF and control conditions. (*C*) Number of layer 5 neurons produced under GOF and control conditions. (*D*) Number of layer 6 neurons produced in GOF and control conditions. (*E*) Fraction of infragranular layer neurons produced under GOF and control conditions. (*F*) Consequences of the experimentally observed variations in TG1 and cell-cycle reentry on the post-mitotic neurons numbers.

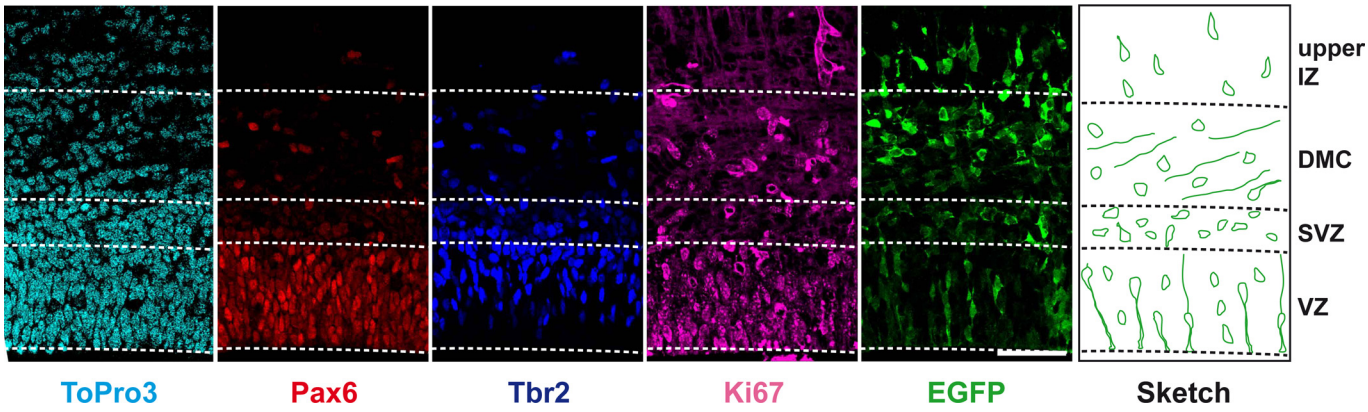

Fig. S9. Criteria used for the establishment of boundaries between different compartments at E17. Nuclear staining with ToPro3 and immunostaining against Pax6, Tbr2, Ki67, and GFP, on a coronal section of mouse embryonic brain (E17), in the dorsal cortex, after electroporation at E15. Limits between compartments were established on cytological cues, immunoreactivity to Pax6, Tbr2, and Ki67, and morphology of GFP+ cells. The VZ corresponds to a dense compartment, showing a neuroepithelial organization, that exhibits high Pax6 and Ki67 immunoreactivity lining the border of the ventricle, in this compartment, Tbr2 cells show a radial orientation. The SVZ is an equally dense compartment, located basally to the VZ, that exhibits high Tbr2 immunoreactivity and where the cells are oriented more tangentially. The DMC is located in the lower part of the IZ. The DMC cell density is low, due to tangentially oriented axonal fibers. A significant amount of DMC cells exhibit Ki67 immunoreactivity and are oriented radially as well as tangentially. Regarding EGFP labeling, VZ cells display the typical radial glial cell and short neural precursors morphology. SVZ cells show the multipolar morphology of BPs. Some DMC cells have the morphology of cells undergoing radial migration, others are oriented tangentially among axonal fibers. (Scale bar, 50 μm.)

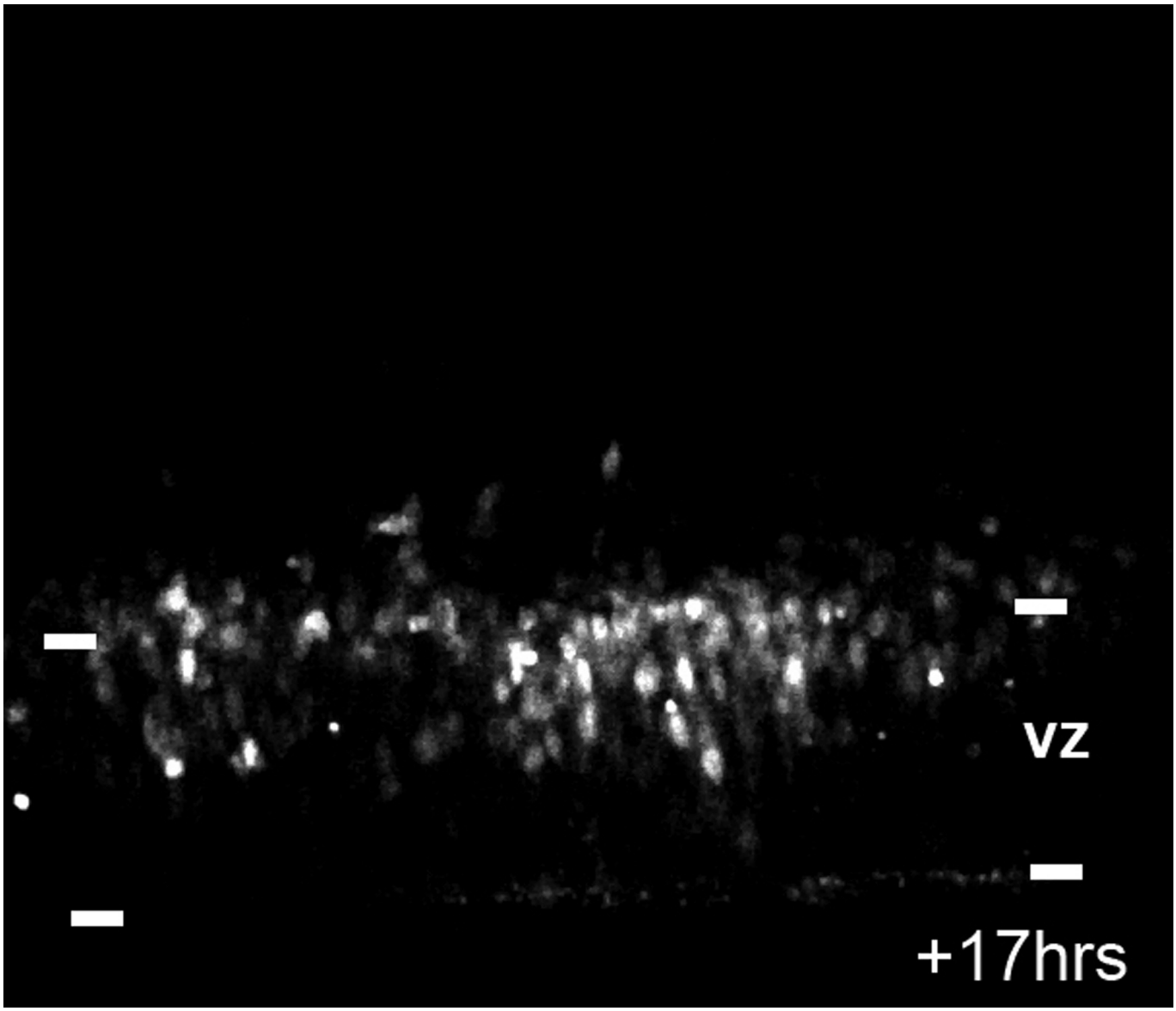

Movie S1. Cohort of EGFP-expressing cells after in utero electroporation in the VZ.

Movie S1 (WMV)

Table S1. Thickness of the VZ and the SVZ at E17, following electroporation at E15, in control and GOF electroporated regions and the strictly homologous region of the contralateral hemisphere, measured on 20 micron thick coronal sections

			VZ thickness (μm)			SVZ thickness (μm)		
Condition	brain	section	nonelectroporated	electroporated	variation, %	nonelectroporated	electroporated	variation, %
Control	1	1	76	73	−4.5	63	78	+24.5
		2	65	67	+3.4	66	59	−10.0
	2	1	67	76	+14.2	57	71	+23.5
		2	70	76	+9.1	75	66	−11.4
	3	1	60	62	+3.2	53	48	−10.5
GOF hCycE	1	1	72	75	+3.4	39	62	+58.4
		2	64	71	+10.3	38	44	+15.5
	2	1	112	95	−15.1	73	99	+35.1
		2	100	94	−5.9	62	119	+94.0
	3	1	71	67	−6.5	43	63	+47.4
GOF mCycD1	1	1	97	101	+4.5	70	83	+18.8
		2	105	97	−7.0	73	92	+26.0
	2	1	67	55	−17.9	56	61	+8.7
		2	72	66	−8.2	50	57	+15.2
	3	1	75	74	−2.3	48	61	+26.8

Comparison of control electroporated and nonelectroporated region showed no statistical difference in the thickness of the VZ or the SVZ.